



# Multifunctionalized carbon-fiber-reinforced polyetheretherketone implant for rapid osseointegration under infected environment

Xiao Wang<sup>a,b,1</sup>, Lisha Pan<sup>a,b,1</sup>, Ao Zheng<sup>a,b</sup>, Lingyan Cao<sup>a,b</sup>, Jin Wen<sup>a,b</sup>, Tingshu Su<sup>a,b</sup>, Xiangkai Zhang<sup>b</sup>, Qingfeng Huang<sup>a,b,\*\*</sup>, Xinquan Jiang<sup>a,b,\*</sup>

<sup>a</sup> Department of Prosthodontics, Shanghai Ninth People's Hospital, Shanghai Jiao Tong University School of Medicine, College of Stomatology, Shanghai Jiao Tong University, 639 Zhizaoju Road, Shanghai, 200011, China

<sup>b</sup> National Center for Stomatology, National Clinical Research Center for Oral Diseases, Shanghai Key Laboratory of Stomatology, Shanghai Engineering Research Center of Advanced Dental Technology and Materials, 639 Zhizaoju Road, Shanghai, 200011, China

## ARTICLE INFO

### Keywords:

Polyetheretherketone  
Nanopores  
Osteogenic activity  
Vascularization  
Antibacterial activity

## ABSTRACT

Carbon fiber reinforced polyetheretherketone (CFRPEEK) possesses a similar elastic modulus to that of human cortical bone and is considered as a promising candidate to replace metallic implants. However, the bioinertness and deficiency of antibacterial activities impede its application in orthopedic and dentistry. In this work, titanium plasma immersion ion implantation (Ti-PIII) is applied to modify CFRPEEK, achieving unique multi-hierarchical nanostructures and active sites on the surface. Then, hybrid polydopamine (PDA)@ZnO-EDN1 nanoparticles (NPs) are introduced to construct versatile surfaces with improved osteogenic and angiogenic properties and excellent antibacterial properties. Our study established that the modified CFRPEEK presented favorable stability and cytocompatibility. Compared with bare CFRPEEK, improved osteogenic differentiation of rat mesenchymal stem cells (BMSCs) and vascularization of human umbilical vein endothelial cells (HUVECs) are found on the functionalized surface due to the zinc ions and EDN1 releasing. *In vitro* bacteriostasis assay confirms that hybrid PDA@ZnO NPs on the functionalized surface provided an effective antibacterial effect. Moreover, the rat infected model corroborates the enhanced antibiosis and osteointegration of the functionalized CFRPEEK. Our findings indicate that the multilevel nanostructured PDA@ZnO-EDN1 coated CFRPEEK with enhanced antibacterial, angiogenic, and osteogenic capacity has great potential as an orthopedic/dental implant material for clinical application.

## 1. Introduction

Polyetheretherketone (PEEK) has been regarded as the prime candidate for orthopedic and dental material owing to its excellent mechanical properties, good biocompatibility, chemical stability, and natural radiolucency [1–4]. Carbo-fiber-reinforced PEEK (CFRPEEK), by modifying short carbon fiber into PEEK, not only inherits excellent properties from PEEK but also obtains appropriate elastic modulus similar to that of human cortical bone which can avoid the complications caused by stress shielding [5]. However, although mechanically

more favorable for implant applications, CFRPEEK has a relatively bioinert surface due to its low surface energy and stable chemical structure, which leads to poor osseointegration [6,7]. In addition, pristine CFRPEEK has a higher bacterial implant infection rate as a result of lacking antibacterial ability, which is more obvious when used in complex oral environment [8–10]. Once postoperative bacterial infection occurs, patients have to suffer from implant replacement surgery and chronic and/or relapsing diseases followed by the failure of the prosthetic implant. Therefore, novel strategies that will endow CFRPEEK with a bionic surface to promote both good antibacterial properties and

Peer review under responsibility of KeAi Communications Co., Ltd.

\* Corresponding author. Department of Prosthodontics, Ninth People's Hospital affiliated to Shanghai Jiao Tong University, School of Medicine, Shanghai, 200011, China..

\*\* Corresponding author. Department of Prosthodontics, Ninth People's Hospital affiliated to Shanghai Jiao Tong University, School of Medicine, Shanghai, 200011, China.

E-mail addresses: [hqfyy@163.com](mailto:hqfyy@163.com) (Q. Huang), [xinquanjiang@aliyun.com](mailto:xinquanjiang@aliyun.com) (X. Jiang).

<sup>1</sup> These authors contributed equally to this work.

<https://doi.org/10.1016/j.bioactmat.2022.12.016>

Received 19 September 2022; Received in revised form 17 December 2022; Accepted 18 December 2022

2452-199X/© 2022 The Authors. Publishing services by Elsevier B.V. on behalf of KeAi Communications Co. Ltd. This is an open access article under the CC BY-NC-ND license (<http://creativecommons.org/licenses/by-nc-nd/4.0/>).

osseointegration abilities are in great need.

In recent years, various strategies have been proposed to develop implants with antibacterial surfaces to inhibit implant-associated infections. The frequently used antimicrobial agents contain metal ions (e.g., Zinc ion ( $Zn^{2+}$ ) [11], silver ion ( $Ag^+$ ) [12], copper ion ( $Cu^{2+}$ ) [13]), halogen elements (e.g., fluorine [14]), antibiotics (e.g., vancomycin [15]) and so on have been proposed [16–18]. Due to their good biodegradability, marked antimicrobial activity and modest cost, zinc oxide nanoparticles (ZnO NPs) are becoming one of the most promising inorganic antimicrobial materials, especially in the field of tissue regeneration [19–23]. Studies have demonstrated quite efficient antimicrobial activity of ZnO NPs against gram-positive and gram-negative bacteria by forming reaction oxygen species (ROS) and releasing zinc ions to damage bacterial cell membranes [24,25]. Besides, zinc has been proven to be the structural or functional component of several key proteins, which can promote osteogenic behavior and stimulate new bone formation by enhancing cell proliferation, differentiation and osteo-related gene expression [5,26]. Furthermore, in addition to being a good source of zinc, ZnO NPs with small particle size can be used as good drug carriers of drugs or factors to improve the biological activity of biomaterials due to their high specific surface area [27,28]. However, efficient antimicrobial abilities usually go along with cytotoxicity. The enriched  $Zn^{2+}$  on the surface can reversely hinder sufficient angiogenic and osteogenic activities of the implant [29–31]. Therefore, the search for balancing antimicrobial activities accompanied by a certain degree of cytotoxicity and osteo-associated activities is of great importance. Based on that, the construction of a multifunctional implant system integrating both excellent antibacterial and osteogenic properties is highly desirable.

Previous literature evidence indicated that early-stage osseointegration was critical for preventing bacteria from adhesion and colonization onto the biomaterial implant surface [32]. Despite advancing antibacterial properties, prompt good osseointegration itself is actually a prerequisite for the success of implantation, which is essential for implants to achieve both initial higher levels of bone anchorage and long-term functionalization [33–35]. When implanted *in vivo*, biomaterial could successively trigger a series of biological reactions with the crucial help of rapid vascularization that is conducive to early-stage bone deposition [36,37]. Angiogenesis can transport essential oxygen and nutrients and induce the accumulation of cells and osteoinductive growth factors to participate in bone remodeling [38,39]. Endothelin-1 (EDN1) is a pro-angiogenic 21 amino acid peptide that can recruit and promote human umbilical vein endothelial cells (HUVECs) proliferation and migration [40–42]. Moreover, our previous studies demonstrated that EDN1 overexpressed bone mesenchymal stem cells (BMSCs) showed a significant increase in proliferation and osteogenesis, and a higher bone mineral density and trabecular number was observed in new bone formation [43]. Therefore, by modifying the surface of CFRPEEK with EDN1, we hope to improve early vascularization and osteogenesis simultaneously and achieve an osseointegration-friendly microenvironment.

Herein, we developed a novel multifunctional CFRPEEK implant with the purpose of combating pathogenic bacteria, inducing angiogenesis, and promoting osteogenesis (Scheme). Firstly, specific multi-hierarchical nanostructures and active sites, in which nanoparticles and nanopores coexist, were constructed by titanium plasma immersion ion implantation (Ti-PIII). We speculate that the increased surface area and active groups were beneficial for the subsequent modification of functional factors. Subsequently, hybrid polydopamine (PDA) @ZnO NPs was modified onto CFRPEEK via PDA-assisting covalent immobilization. Through introducing the covalently immobilized PDA-nanoparticle coating, ZnO NPs were distributed uniformly in the self-assembled PDA coating and stably immobilized on the CFRPEEK surface to achieve long-lasting antibacterial activity and reduce cytotoxic actions along with the efficient antimicrobial actions. To balance the antimicrobial influence on osseointegration-associated activities, we

further incorporated pro-angiogenic EDN1 onto the antibacterial surface thanks to the superior adhesive property of PDA. Through this "anti-bacterial/angiogenic/osteogenic" integrated strategy, we aimed to develop a novel method to improve the anti-infection performance and osteogenic ability of CFRPEEK implants, which may inspire well-founded hopes to spur the development of PEEK implants in the field of orthopedics or dentistry, and provide a new strategy for implant modification with a comprehensive therapeutic effect of preventing infection superactively and promoting vascularized bone regeneration effectively.

## 2. Materials and methods

### 2.1. Sample preparation

All samples were machined from biomedical grade carbon-fiber-reinforced polyetheretherketone (CFRPEEK) with 30% (v/v) carbon fibers and then polished and ultrasonically cleaned before plasma immersion ion implantation (PIII). Then, titanium ions were implanted into CFRPEEK samples via a filtered cathodic arc source to prepare Ti-PIII samples. ZnO nanoparticles were synthesized by sol-gel method and then mixed with equivalent dopamine (1:1) in Tris-HCl (PH 8.5). Afterward, Ti-PIII samples were immersed and stirred in the solution mentioned above in dark for 12 h, ultrasonically cleaned with distilled water for 3 times, and finally prepared into the hybrid PDA@ZnO nanoparticles modified surface (Ti-PIII/PDA@ZnO). Then, 50  $\mu$ L of EDN1 solution (300  $\mu$ g mL<sup>-1</sup>) was dropped onto the Ti-PIII/PDA@ZnO plates and all plates were placed in a vacuum air pump for vacuum drying. Finally, the EDN1 treated samples were washed with deionized H<sub>2</sub>O to remove unadsorbed protein. The prepared eventual samples were denoted as Ti-PIII/PDA@ZnO-EDN1.

### 2.2. Surface structure and chemical characterization

Surface morphologies of different samples were observed by field-emission scanning electron microscopy (FE-SEM, Hitachi S-4800, Japan). The elemental compositions and mappings of the Ti-PIII/PDA@ZnO-EDN1 sample were determined by energy-dispersive X-ray spectrometry (EDS, EPMA, JAX-8100, Japan). The wettability of different samples was examined by water contact angle measurement. Additionally, the surface mechanical properties of the modified samples were characterized by the Vickers hardness instrument.

### 2.3. Ion release

For the detection of Ti and Zn ion release, each sample was immersed in 1 mL phosphate buffered saline (PBS) at 37 °C for different immersion time (7, 14, 21, 28 days). At a prescribed time, the extracts were collected and analyzed by inductively-coupled plasma atomic emission spectroscopy (ICP-AES, JY 2000-2, France).

### 2.4. Release kinetics of EDN1 *in vitro*

Briefly, Ti-PIII/PDA@ZnO-EDN1 samples were incubated in a microcentrifuge tube containing 1 ml PBS at 37 °C and the supernatant was collected at each selected time points (0, 1, 3, 5, 7, 14, 21, 28 days) and stored at –80 °C. Finally, the release of EDN1 was measured using enzyme-linked immunosorbent assay (ELISA) kits (BD Bioscience, San Jose, CA, USA).

### 2.5. Fibronectin adsorption on surfaces

Cell responses to the implant surface occur after protein adsorption from physiological solutions and the surface properties significantly affect protein adsorption. In this study, ELISA was used to measure the amount of fibronectin adsorbed on different CFRPEEK surfaces. Samples

were incubated in a 24-well plate containing 1 mL Dulbecco's modified Eagle medium (DMEM) with 10% fetal bovine serum (FBS) for 1 and 4 h at 37 °C and then treated with mouse monoclonal anti-fibronectin primary antibody (Santa Cruz Biotechnology, dilution, 1:50) and anti-mouse secondary antibody conjugated with horseradish peroxidase (HRP, Bio-Rad, MD, USA). The results were shown as units of optical density (OD) absorbance value.

## 2.6. Biocompatibility experiments in vitro

Bone marrow-derived mesenchymal stem cells (BMSCs) used in this study were obtained from the SD rat femur. BMSCs were cultured in high glucose DMEM (10% FBS, 100 µg mL<sup>-1</sup> streptomycin, and 100 U mL<sup>-1</sup> penicillin) at 37 °C with 5% CO<sub>2</sub> in the incubator. The medium was changed every three days. BMSCs of the second passage were used in all experiments.

### 2.6.1. BMSCs adhesion on samples

For cell adhesion detection, the expression of integrin β1 after initial seeding was measured. At the protein level, cells were fixed after 12 h of incubation and detected using the immunofluorescence method. Briefly, a specific primary antibody targeting integrin β1 and vinculin (Abcam, Cambridge, UK) and DyLight 488-conjugated anti-mouse IgG antibody were used to detect the expression of integrin β1 and vinculin in the experiment. The cell cytoskeleton and nuclei were stained with TRITC-phalloidin (Enzo Life Science Ltd, Exeter, UK) and 4',6-diamidino-2-phenylindole (DAPI) (Invitrogen, Carlsbad, CA, USA), respectively. At the genetic level, total RNA was collected at 4 and 12 h, and the expression levels of adhesion-related genes (Integrin β1, Integrin α2, Vinculin) were measured by RT-PCR (primers were displayed in Table S1).

### 2.6.2. BMSCs proliferation on samples

Counting Kit-8 (CCK-8, Dojindo Laboratories Inc., Kumamoto, Japan) assay was used to investigate the proliferation of BMSCs on modified CFRPEEK substrates. Briefly, BMSCs were seeded on samples and incubated for 1, 4 and 7 days respectively before the CCK-8 assay. Meanwhile, to further examine the activity of DNA replication in BMSCs, an EdU assay was used to label BMSCs on modified substrates at 48 h and then examined by confocal laser scanning microscope (CLSM).

## 2.7. BMSCs osteogenic differentiation on modified samples

To investigate the early osteogenic differentiation ability, BMSCs were firstly fixed after 4 and 7 days of incubation on different plates and then stained with an ALP kit (Beyotime, Shanghai, China). Meanwhile, p-nitrophenyl phosphate (pNPP) (Sigma, St Louis, MO, USA) was used to perform ALP quantitative assay. Calcium deposition was further performed after BMSCs were cultured for 14 days in DMEM. BMSCs were firstly fixed and then stained using 1% Alizarin Red (Sigma-Aldrich) for 10 min, and rinsed with PBS. The nuclei were counterstained with DAPI, and calcium deposition was observed by LSCM. Afterward, the stained samples were detached from 10% cetylpyridinium chloride (Sigma) solution and the OD values were quantitatively detected at 590 nm.

Then, the expression of OCN and OPN was detected by immunofluorescence method after 7-day incubation. Moreover, RT-PCR was performed to investigate the relative gene expression level. 1 × 10<sup>5</sup> BMSCs were seeded on various samples (20 mm × 20 mm × 1 mm) in 6-well plates. After each prescribed point time (4 and 7 days) of culture, the total RNA of BMSCs on different samples was extracted using the Trizol reagent (Invitrogen, Carlsbad, USA). Gene expression of runt-related transcription factor 2 (Runx2), alkaline phosphatase (Alp) at the early stage (4 days) and osteocalcin (Ocn), osteopontin (Opn), bone sialoprotein (Bsp), osterix (Osx) at the late stage (7 days) were detected by RT-PCR system (primers were displayed in Table S1).

## 2.8. In vitro angiogenesis assay

### 2.8.1. Migration assay of HUVECs

Wound healing assay was used to examine the migration activity of human umbilical vein endothelial cells (HUVECs) (AllCells, Shanghai, China). Cells (1 × 10<sup>5</sup> per well) were seeded onto different samples and starved overnight in DMEM without FBS, and then wounded carefully with a plastic pipette. After another 12 and 24 h of incubation, the samples were fixed and then stained with both Rhodamine-phalloidin (Enzo Life Sciences, Exeter, UK) and DAPI. Images of all specimens were recorded by CLSM (Leica, Hamburg, Germany). The areas between the cell layer borders were calculated via Image J.

### 2.8.2. Recruitment capacity of HUVECs

Transwell assay was used to investigate the recruitment capacity of different samples on HUVECs. Each sample was placed in the lower chambers of the transwell plates with 8 µm pore membranes, of which had HUVECs in their upper chambers. After 12 and 24 h, HUVECs penetrated the membranes of the upper chambers were fixed and investigated under a microscope.

### 2.8.3. Tube formation assay

Endothelial tube formation assay was used to examine the angiogenesis ability of HUVECs on different samples. 50 µL matrigel (Millipore, Cat. No. ECM625) was transferred to each well of a 96-well plate and then cultured in a 37 °C incubator for 30 min to form a gel. Then HUVECs co-cultured with different samples in advance at a density of 1 × 10<sup>4</sup> cells/well were added and incubated on the surface of the matrigel.

After 6 h of incubation, cells were recorded by inverted light microscope (Leica DMI 3000B, Germany) from five random microscopic fields. Nodes, master junction, meshes, and segments were referred as parameters of the gradual regeneration process of angiogenesis.

### 2.8.4. Expression of angiogenesis-related genes

The gene expression of vascular endothelial growth factor (VEGF) and hypoxia-inducible factor 1α (HIF-1α) in HUVECs co-cultured with different samples was detected at 4 days. The sequences of different primers were displayed in Table S1.

## 2.9. In vitro antibacterial activity

*Staphylococcus aureus* (*S. aureus*, ATCC 25923) and *Escherichia coli* (*E. coli*, ATCC 25922) cultured in MHB (Mueller-Hinton Broth) medium were used for the antibacterial assay. Briefly, 500 µL bacteria suspension (1 × 10<sup>6</sup> CFU mL<sup>-1</sup>) was incubated with different samples in 24-well plates at 37 °C for 6 h.

### 2.9.1. Live/dead fluorescence staining assay

To qualitatively evaluate the bacteria viability, bacteria were co-cultured with modified substrates for 12 h and stained with a Live/Dead (green/red) BacLight bacteria viability kit (Invitrogen), followed by observation under CLSM.

### 2.9.2. Bacteria counting test

The spread plate method was used to evaluate the antibacterial ratio of different samples. Firstly, different samples were washed with PBS and then soaked in 1 mL sterile PBS. Secondly, bacteria adhered to sample surface were ultrasonically detached for 5 min. 100 µL mixture solution was spread onto agar plates and then incubated at 37 °C for 12 h. Finally, the number of active colonies formed units (CFUs) was counted and imaged.

## 2.10. Investigation of antibacterial mechanism

### 2.10.1. ROS detection

1,3-Diphenylisobenzofuran (DPBF) was used to investigate the ROS generation of different samples. Briefly, all the samples were incubated with 500  $\mu\text{L}$  DPBF solution (20  $\mu\text{g mL}^{-1}$  dissolved in DMSO) for 5 min. The extracts were collected for absorbance detection under UV–vis.

### 2.10.2. Membrane permeability assay

O-nitrophenyl- $\beta$ -D-galactopyranoside (ONPG) assay was used to evaluate bacterial membrane permeability on different substrates. Briefly, 500  $\mu\text{L}$  bacterial suspension ( $1 \times 10^6$  CFU  $\text{mL}^{-1}$ ) was incubated with different samples at 37  $^{\circ}\text{C}$  for 6 h. Afterward, bacteria adhered on sample surfaces were soaked with 500  $\mu\text{L}$  ONPG solution (0.75  $\text{M}$  in  $\text{NaH}_2\text{PO}_4$  buffer, pH 7.0). The absorbance of the supernatant was recorded by spectrophotometric microplate reader (Bio-Rad 680, USA) at 405 nm.

### 2.10.3. ATP level test

ATP level of bacteria adhered on different samples was used to estimate the metabolic level of bacteria. Briefly, 500  $\mu\text{L}$  bacterial suspension ( $1 \times 10^6$  CFU  $\text{mL}^{-1}$ ) was incubated with different samples at 37  $^{\circ}\text{C}$  for 6 h, and then the ATP levels were measured by luminescence intensity via an Enhanced ATP Assay Kit (Beyotime) according to the experimental instruction.

## 2.11. In vivo study

All surgical experiments were approved by Animal Ethics Committee of Shanghai Jiao Tong University and animals were randomly divided into three groups (Ti-PIII, Ti-PIII/PDA@ZnO, Ti-PIII/PDA@ZnO-EDN1). To construct a bacterial infection implant model, different implants were immersed in *S. aureus* bacteria inocula ( $2 \times 10^3$  CFUs), and then samples were removed to a wet environment, followed by sterile operation. Briefly, SD rats were anesthetized before operating. The femur near the knee joint was exposed through the incision, and a narrow channel was created at the femoral condyle by surgical drill (1.2 mm in diameter). Finally, the skin and soft tissue were sutured carefully. And then, the process of new bone formation and mineralization was assessed by a polychrome sequential fluorescent labeling method. Different fluorochromes were administered intraperitoneally at a sequence of 30  $\text{mg kg}^{-1}$  Alizarin Red S (Sigma, USA) and 20  $\text{mg kg}^{-1}$  Calcein (Sigma) at 2 and 4 weeks after the operation, respectively.

### 2.11.1. In vivo antibacterial efficiency and biosafety evaluation

Twelve rats were sacrificed 6 weeks after implantation, and the rods (3 rods per group) were gently removed into the tuber with 1 mL PBS. To detach all adhered bacteria, the extracts were sonicated for 10 min and diluted with PBS. Next, 100  $\mu\text{L}$  diluents of different groups were added and spread onto agar plates and cultured at 37  $^{\circ}\text{C}$  for 12 h. Finally, the visible bacterial colonies were recorded and imaged. In addition, to observe the turbidity of the medium, the different treated rods were further soaked with 3 mL MHB medium and co-cultured at 37  $^{\circ}\text{C}$  for 12 h. At the same time, the remaining femurs without implants were gently obtained and fixed in formaldehyde solution (4%) at 4  $^{\circ}\text{C}$  for 72 h, followed by serially dehydrated with ethanol solution (50%, 70%, 90%, 100%, and 100%), infiltrated with xylene and embedded with paraffin. Finally, paraffin slices of tissues around implants were investigated to evaluate the infection status by H&E staining.

Moreover, to examine the biosafety of the Ti-PIII/PDA@ZnO-EDN1 antibacterial system, major organs including heart, liver, kidney, lung and spleen were histologically evaluated after implantation for 6 weeks. Briefly, these organs were fixed in 4% paraformaldehyde and then serially dehydrated with ethanol solution, infiltrated with xylene, and embedded with paraffin, respectively. Finally, H&E staining was performed to observe the metabolism of nanoparticles.

### 2.11.2. Micro-CT analysis

Micro computed tomography scanning was used to investigate the osseointegration and vascularization of the bone-implant interface. Before all rats were sacrificed, four rats from each group were randomly chosen for vascular perfusion via the abdominal aorta using Microfil (Flow Tech, USA). Then the femurs with implants were harvested and fixed in 10% buffered formaldehyde for Micro-CT. Affiliated analyzing software was used to reconstruct the obtained scanning of 2D images into 3D images. After reconstruction, the percentage of new bone volume to tissue volume (BV/TV) and bone mineral density (BMD of BV) were quantitated.

Samples processed with Microfil were decalcified in 10% Ethylene Diamine Tetraacetic Acid (EDTA) for approximately 2 months to evaluate blood vessel formation. A region with a radius of 1 mm around the implant was examined for new vascularization.

### 2.11.3. Histological observation

The different harvested tibia implants were respectively fixed with 4% paraformaldehyde, serially ascending dehydrated with ethanol solution, and infiltrated with xylene and embedded in poly (methyl methacrylate). The undecalcified sections were plane-parallelly to the long axis containing the implant central of each implant by microtome (SP1600, Leica, Germany). For fluorescence labeling observation, sections were subsequently ground and polished to a thickness of about 40 mm. Excitation/emission wavelengths of chelating fluorochromes were used 543/617 nm and 488/517 nm for Alizarin Red S (red) and Calcein (green), respectively. Finally, after being stained with Van Gieson's picrofuchsin, sections revealed the mineralized bone tissue and were then recorded by inverted microscope (Olympus, Japan).

The decalcified samples were embedded in paraffin, and cut into 4  $\mu\text{m}$  slices, followed by CD31 immunohistochemical staining.

## 2.12. Statistical analysis

All data were presented as mean  $\pm$  standard deviation (SD). Statistical analysis was performed with one-way analysis of variance (ANOVA) followed by Tukey's post hoc test for multiple comparisons using GraphPad Prism 8.0 statistical software package. Values of \* $p < 0.05$  and \*\* $p < 0.01$  were considered to be statistically significant.

## 3. Results and discussion

### 3.1. Fabrication and characterization of multifunctional CFRPEEK surfaces

We developed a novel multifunctional implant (Ti-PIII/PDA@ZnO-EDN1) with the purpose of inducing angiogenesis, promoting osteogenesis, and combating pathogenic bacteria. Surface morphologies of different modified surfaces were characterized by scanning electron microscope (SEM). As shown in Fig. 1A, nanopores were uniformly formed on the surface of CFRPEEK substrates after Ti-PIII, and small nanoparticles were further observed fully covering all walls of the nanopores at higher magnification. The result was consistent with our previous study. Through PDA-assisting covalent immobilization, hybrid PDA@ZnO nanoparticles were decorated onto the substrate evenly. The successful fabrication of uniform and stable modified layer mainly attributes to the multi-nanostructures on the CFRPEEK surface. Owing to the high surface area to volume ratio, nanopores could serve as an efficient interface for rapid nucleation and provide more sites for the ordered growth of ZnO nanoparticles. Moreover, as the hydroxyl groups ( $-\text{OH}$ ) attached to the benzene ring of dopamine are strong titanium chelation, hybrid PDA@ZnO coatings can chelate titanium dioxide ( $\text{TiO}_2$ ) nanoparticles distributed on Ti-PIII surface during dopamine self-polymerization [44,45], thus effectively improving the combining efficiency of hybrid PDA@ZnO nanoparticles on CFRPEEK surface. Accordingly, preparing the Ti-PIII surface is of great necessity for

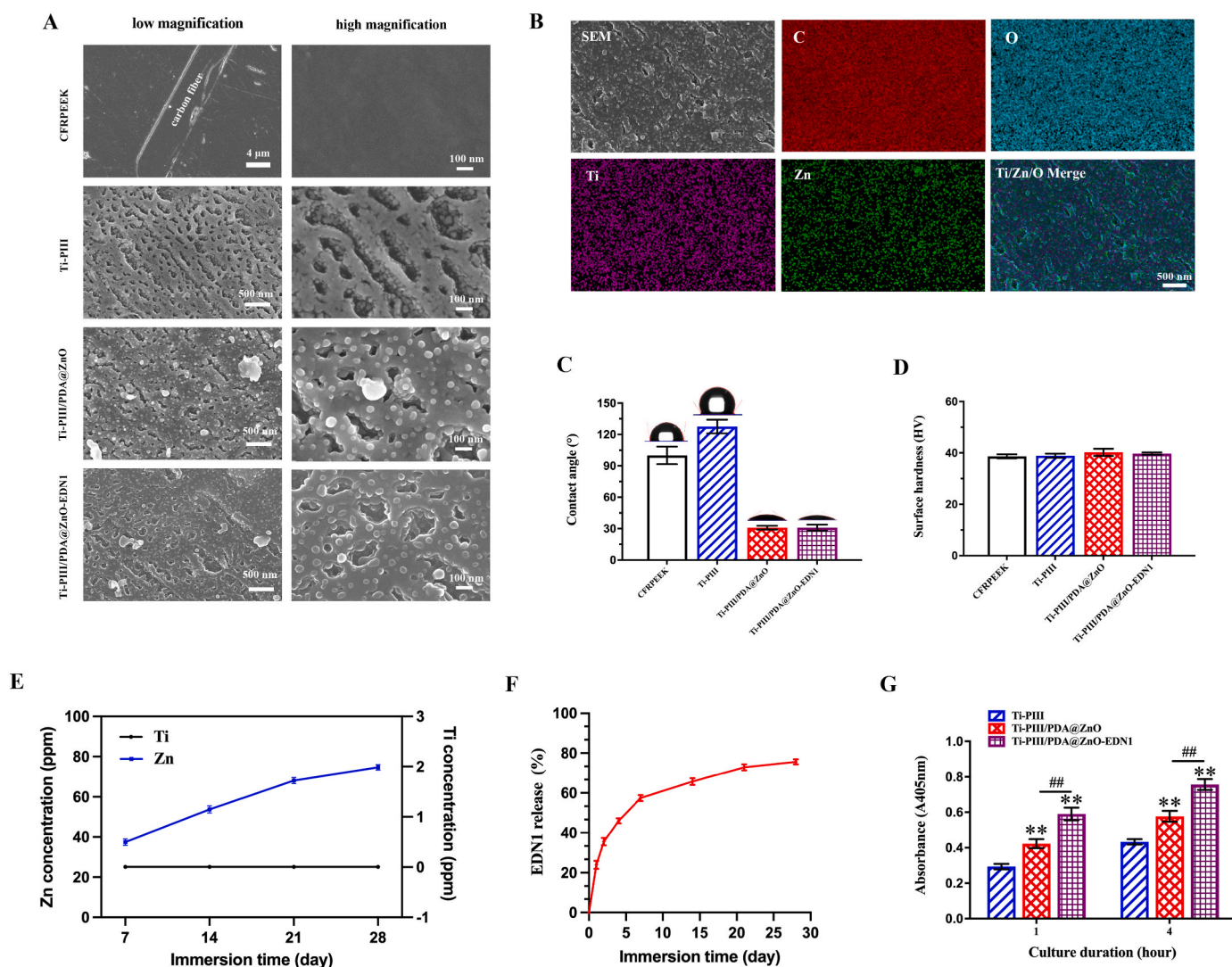


**Fig. 1.** Surface microstructures of the coatings. A) Surface microstructures of the CFRPEEK before and after Ti-PIII and hybrid PDA@ZnO NPs (or PDA@ZnO-EDN1) treatment. B) Energy-dispersive X-ray mapping of the Ti-PIII/PDA@ZnO-EDN1 surface. C) Water contact angles and photographs of water droplets on different samples. D) Vickers hardness of different samples. E) Ti and Zn ions concentration after immersion for different time. F) The release of EDN1 protein after immersion for different time. G) Increased fibronectin adsorption on modified surfaces. \* $p < 0.05$ , \*\* $p < 0.01$  when compared with Ti-PIII; # $p < 0.05$ , ## $p < 0.01$  when Ti-PIII/PDA@ZnO-EDN1 compared with Ti-PIII/PDA@ZnO.

promoting hybrid PDA@ZnO nanoparticles growth rather than native CFRPEEK.

According to the energy-dispersive X-ray spectroscopy (EDS) elemental mapping analysis (Fig. 1B), an even overlay of Ti and Zn was detected on modified surfaces. Further up, the trace element release was investigated by using the inductively-coupled plasma atomic emission spectroscopy (ICP-AES, JY 2000-2, France) analysis. As shown in Fig. 1E, there was no obvious release of Ti ions on modified surfaces, while the incorporated Zn ions were continuously released within 28 days. In conclusion, SEM, EDS, and ion release characterization verified that the prepared Ti-PIII/PDA@ZnO implants integrated multi-hierarchical nanostructures and active ion components, and might maintain long-term bioactive effects.

Besides, the water contact angle was determined by goniometry to present the hydrophilic/hydrophobic property of the step-by-step modified samples (Fig. 1C). After plasma immersion ion implantation (PIII) treatment, Ti-PIII groups showed strong hydrophobicity according to a contact angle of  $127.5 \pm 6.5^\circ$ , while the contact angle of PDA@ZnO modified groups decreased to  $30.9 \pm 1.8^\circ$  owing to the hydrophilicity of PDA layer. However, after subsequently conjugating with EDN1, the

contact angle showed no obvious change compared with PDA@ZnO modified groups. Therefore, the PDA@ZnO-EDN1 decorated surface had an improved wettability compared with Ti-PIII substrates. Through increasing the affinity between cells and biomaterials, Ti-PIII/PDA@ZnO-EDN1 groups are expected to facilitate cell adhesion and the osteogenic response of bone-related cells.

The mechanical stability of the multi-hierarchical nanostructures on CFRPEEK was further investigated by Vickers hardness measurement. It turned out that there was no difference in Vickers hardness among different groups (Fig. 1D), indicating that the surface mechanical properties were stable enough to avoid being changed by the porous structure produced by ion implantation.

In order to endow CFRPEEK implants with multi-functions, we further introduced EDN1 onto the nanostructured surface through the vacuum method as we previously reported [46]. As shown in Fig. 1A, the covalent immobilized EDN1 did not change the surface morphology of modified PEEK. In addition, the hybrid PDA@ZnO modified surface was more conducive to EDN1 loading (Fig. S1) and the result of factor release (Fig. 1F) showed a slow release of EDN1 sustained for up to 28 days. We speculate that the slow release of EDN1 occurring on the modified

surface is mainly due to the nanopores and hybrid nanoparticles. On one hand, as catechol groups of PDA can react with the amino groups (-NH<sub>2</sub>) of EDN1 through Michael addition or Schiff base reaction, EDN1 molecules will be covalently grafted onto PDA with a greatly improved binding rate. On the other hand, the negative pressure produced by vacuum extraction makes EDN1 protein particles enter into the nanopore structure and accordingly attach to the nanoparticles on the walls

of nanopores. Therefore, the modified surface integrated nanopores and hybrid nanoparticles can be used as an excellent factor delivery system to realize the long-term and slow release of bioactive factors.

Fig. 1G showed that PDA@ZnO modified surfaces significantly promote the adsorption of fibronectin compared to the Ti-PtIII group at both time points, and the EDN1 decorated group has the most obvious protein adsorption effect, which indicates that the multi-functional surface

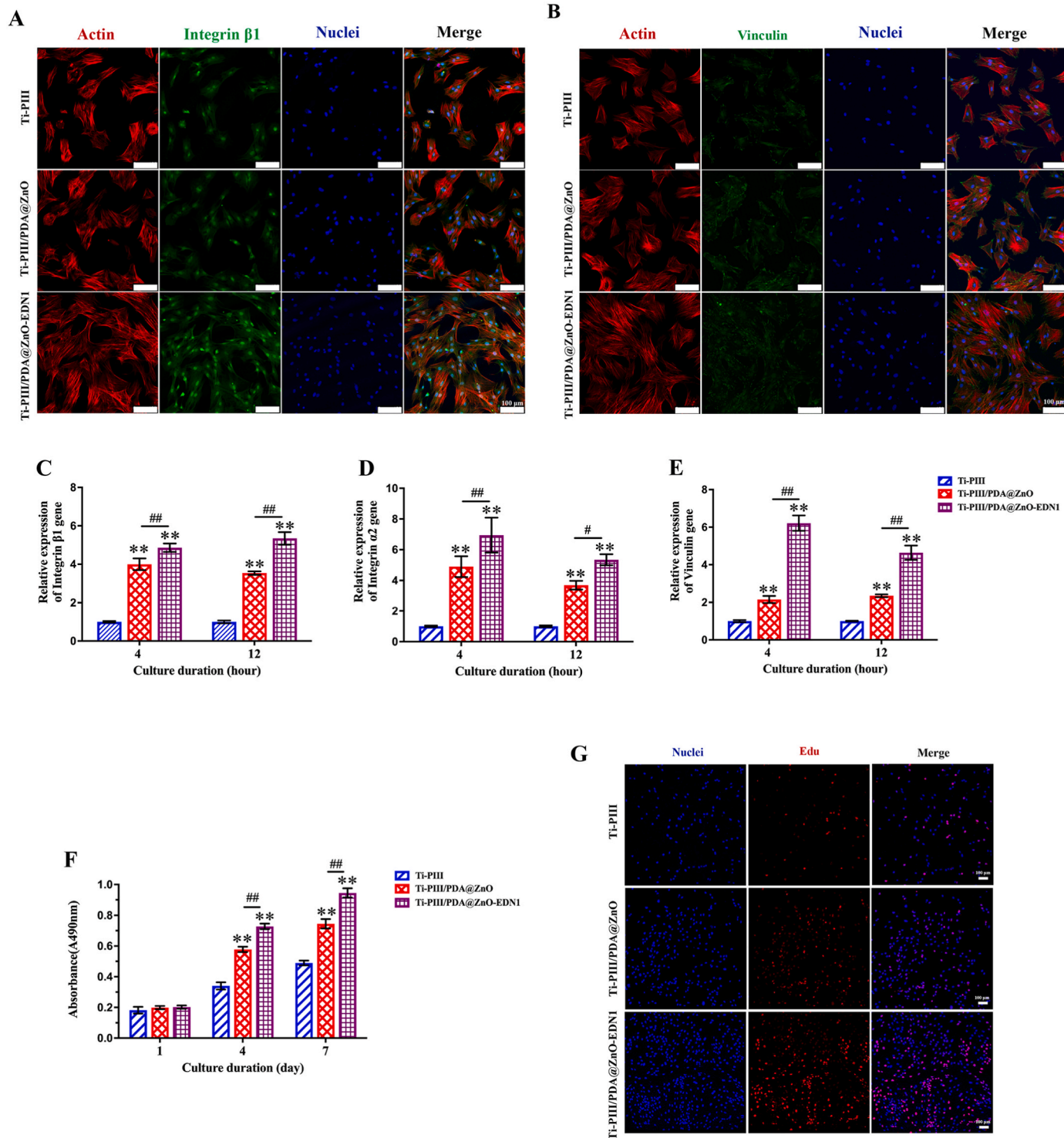


Fig. 2. A, B) The expression of integrin β1 and vinculin at the protein level on different samples. “Merge” represents the merged images of actin (red), protein (green), and nuclei (blue). C ~ E) RT-PCR detection of integrin β1, integrin α2 and vinculin gene expression in BMSCs after incubating on different samples for 4 and 12 h. F) Proliferation activity of BMSCs cultured on different plates for 1, 4, and 7 days. G) Evaluation of BMSCs proliferation at 48 h by EdU staining. \*p < 0.05, \*\*p < 0.01 when compared with Ti-PtIII; #p < 0.05, ##p < 0.01 when Ti-PtIII/PDA@ZnO-EDN1 compared with Ti-PtIII/PDA@ZnO.

favors the initial adsorption of fibronectin.

### 3.2. Response of BMSCs *in vitro*

#### 3.2.1. Cell adhesion and cell proliferation

To verify the possible applications in biomedical research and therapeutics, we investigated the response of BMSCs on different surfaces. To evaluate the effect of modified surfaces on early cell adhesion, the expression of integrin  $\beta 1$  and vinculin was examined after initial seeding. As shown in Fig. 2A, with the EDN1 conjugation, cells expressed the highest levels of integrin  $\beta 1$  in Ti-PIII/PDA@ZnO-EDN1 groups. Vinculin is considered related to the formation of focal adhesion, as it mediates cell adhesion and acts as an adaptor protein of F-actin to participate in filopodia and lamellipodia assembly [47]. Therefore, we fluorescently labeled vinculin, F-actin, and nuclei in BMSCs cultured on different surfaces for 12 h as shown in Fig. 2B. Similarly, the expression of vinculin protein (green) increased remarkably in the hybrid chemicals-modified groups, especially in the EDN1 immobilized group. The further genetic level investigation by real-time polymerase chain reaction (RT-PCR) also displayed a significantly higher expression level of adhesion-related gene integrin  $\beta 1$ , integrin  $\alpha 2$  and vinculin at early time points (4 and 12 h) in two PDA@ZnO modified groups than that in the Ti-PIII group, and the highest expression was observed in the EDN1 immobilized group (Fig. 2C–E). These results were consistent with that at the protein level.

As integrating the multi-hierarchical structure and various bioactive chemicals, we expect that our well-designed multifunctional surface can regulate cell fate and complicated cell behavior at different levels. Hybrid PDA@ZnO nanoparticles with appropriate size were considered to play a key role in early adhesion. Although the control group (Ti-PIII group) also contained TiO<sub>2</sub> nanoparticles produced by Ti-PIII treatment, the particles were limited for particle-cell contact at the early stage of cell adhesion as they distributed in nanopores, in other words, on the interior surface of the substrates. Consequently, we speculate that hybrid PDA@ZnO nanoparticles distributed on the exterior surface of the substrates mainly regulate the initial adhesion of BMSCs. Furthermore, the modified surfaces obtain higher hydrophilicity, which is more conducive to cell adhesion and spreading. Previous research verified that the modified nanostructure could promote BMSCs adhesion through serum protein absorption (such as fibronectin) [48,49]. As shown in Fig. 1G, EDN1 immobilized on the nanostructured surface promoted more fibronectin to aggregate onto the substrates, which may further benefit cell adhesion. Hence, we conclude that in addition to the biological effects, the immobilized EDN1 can also regulate cell adhesion by promoting the aggregation of serum proteins and even exposing more binding sites by unfolding itself on the substrate.

Meanwhile, cell proliferation of BMSCs was investigated by Counting Kit-8 (CCK-8) assay. Generally, cells proliferate time-dependently on different substrates. As shown in Fig. 2F, BMSCs cultured on PDA@ZnO modified samples displayed significantly higher cell viability than the Ti-PIII group after 4 and 7 days of incubation, especially on the Ti-PIII/PDA@ZnO-EDN1 group. A similar tendency occurred in the 5-ethynyl-2'-deoxyuridine (EdU) staining assay (Fig. 2G). After 48 h of incubation, three groups showed obvious differences in terms of cell number, and the EDN1 conjugated group had the most cells and the highest proportion of EdU-positive cells. According to the above results, we infer that by improving the hydrophilicity of nanopores and facilitating initial adhesion and proliferation of BMSCs, the introduced PDA@ZnO and EDN1 ultimately promote cellular compatibility of the modified substrate.

Remarkably, BMSCs on EDN1 modified surface exhibited elongated cell morphology which was considered to be conducive to osteo-differentiation [50,51], and still spread better than the other two groups. Previous study reported that nanoparticles with an average size of 20 nm provided a step-by-step anchor for integrin clustering and focal adhesion contact formation, meanwhile, nanopores could induce cells to

elongate or stretch, to maintain good cell vitality and benefit the up-regulation of osteoblastic expressions [52]. As consistent with the previous research, our result suggests that PDA@ZnO-EDN1 substrates can promote early-stage cell adhesion and spread of BMSCs, which is crucial for the regulation of subsequent proliferation, differentiation, and tissue formation.

#### 3.2.2. Osteogenic bioactivity evaluation of modified surfaces *in vitro*

To enhance the osseointegration of implants, the ideal bio-interface is expected to possess favorable cytocompatibility and effective osteogenic activity. Alkaline phosphatase (ALP) activity assay, calcium deposition staining, gene, and corresponding marker protein expression were conducted to evaluate the effect of modified surfaces towards osteogenic induction. In terms of osteogenic differentiation, Ti-PIII/PDA@ZnO groups obtained significantly enhanced ALP activity and calcium deposition ability compared with Ti-PIII groups, while these osteogenic-differentiation-related activities were further enhanced after incorporating EDN1 in Ti-PIII/PDA@ZnO-EDN1 groups (Fig. 3A–D). At the protein level, the expression of two major osteogenic-differentiation-related markers (OCN and OPN) was detected after 7 days of culturing by immunofluorescence. As shown in Fig. 3E and 3F, the expression of OCN and OPN was higher in Ti-PIII/PDA@ZnO groups than those in Ti-PIII groups, and the highest expression of both markers was found in the EDN1 conjugated group. The osteogenic-differentiation ability of the modified surfaces was further investigated at the genetic level. As shown in Fig. 3G, BMSCs cultured on Ti-PIII/PDA@ZnO-EDN1 groups exhibited the most obvious osteogenic-differentiation tendency by upregulating related markers Runx2 and Alp expression at the early stage (4 days), Ocn, Opn, Bsp and Osx at the late stage (7 days). Overall, the EDN1 conjugated surface significantly stimulated the osteogenic differentiation ability of BMSCs. All these results demonstrated that Ti-PIII/PDA@ZnO-EDN1 groups possess superior capability in promoting *in vitro* osteoblastic maturation attributed to a synergistic effect of multi-hierarchical nanostructures, hybrid PDA@ZnO nanoparticles and EDN1 protein.

### 3.3. Angiogenic activity of modified surfaces *in vitro*

As mentioned in the introduction, it is widely acknowledged that the angiogenic-osteogenic coupling ability might enhance *in vivo* fast osseointegration. To evaluate the effects of the PDA@ZnO-EDN1 coatings on angiogenic behaviors of HUVECs, scratch wound healing, transwell, and *in vitro* tube formation assays were performed. The scratch test (Fig. 4A and 4C) showed that the PDA@ZnO-EDN1 modified group can significantly promote the migration of endothelial cells, which is conducive to the formation of vascular network on the implant surface. The effect of chemical components released from different samples on modulating migration of HUVECs was further evaluated via a co-culture system, and crystal violet staining images were taken after 12 and 24 h (Fig. 4B and 4D). In response to different surfaces, the HUVECs migrated across the transwell permeable membranes, ultimately reaching and adhering to the bottom sides of the membrane. The HUVECs cultured with two PDA@ZnO coating groups responded more to the recruitment of the modified surfaces compared with the pristine Ti-PIII group, while the EDN1 conjugated group obtained the highest recruiting tendency. Similarly, the Ti-PIII/PDA@ZnO-EDN1 groups showed a more significant influence on *in vitro* tube formation of HUVECs compared with the other two groups (Fig. 4E–I)

In order to further explore the underlying mechanisms of angiogenesis that occurred on the modified surfaces, HUVECs directly cultured on different modified substrates were assayed for their expression of angiogenic-related markers at the genetic level, including hypoxia-inducible factor (HIF-1 $\alpha$ ) and vascular endothelial growth factor (VEGF). As shown in Fig. 4J, the EDN1 incorporated coatings had significant regulating effects on the genetic expression of HIF-1 $\alpha$  and VEGF in the adherent cells compared with the other two groups. It has

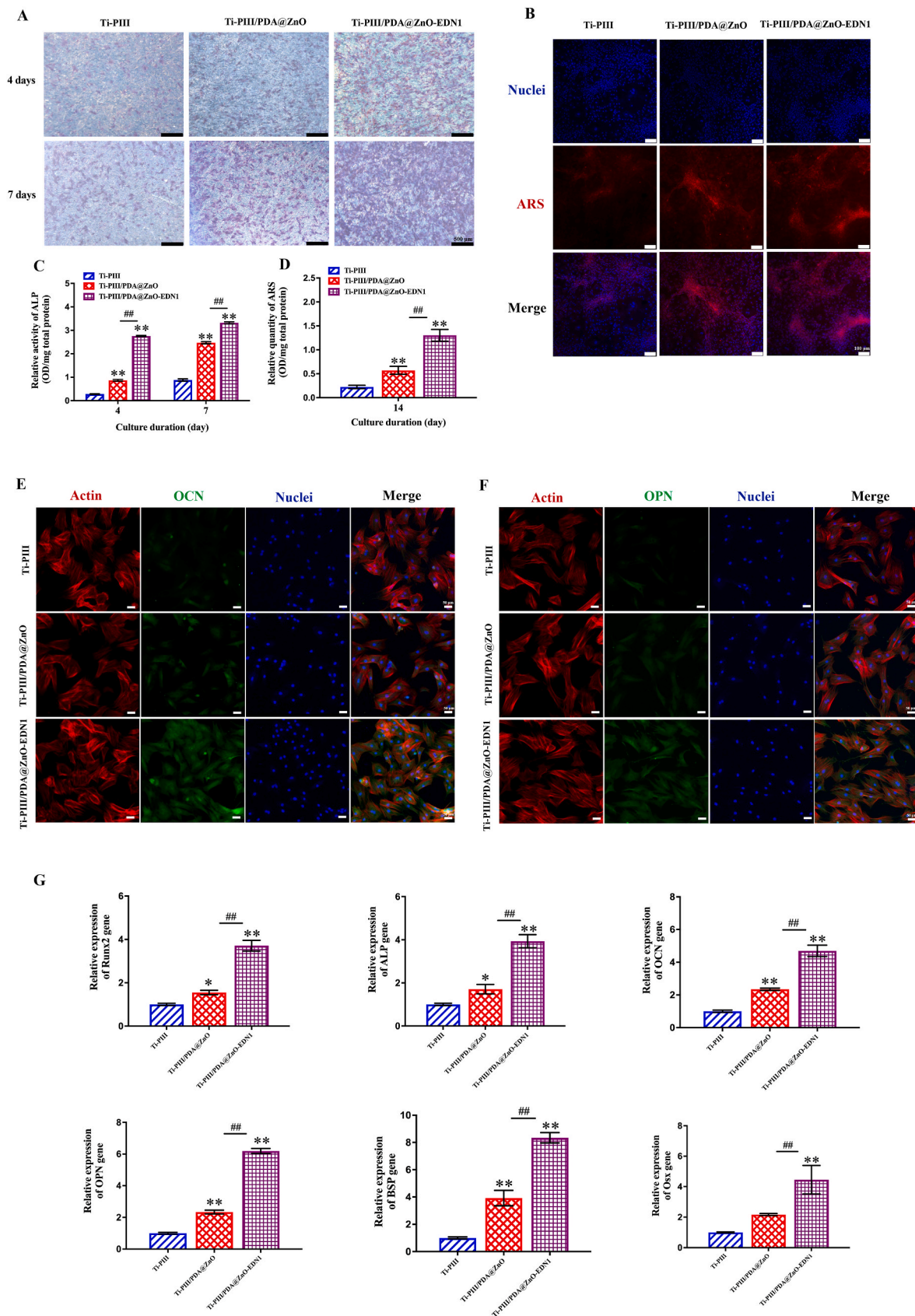


**Fig. 3.** The osteogenic effects of modified surfaces on BMSCs. A) ALP staining of BMSCs cultured on CFRPEEK plates for 4 and 7 days. B) Alizarin Red S (ARS) staining of BMSCs after 14 days of culturing. Red fluorescence represents calcium deposition and the nuclei appear blue. C, D) Quantitative analysis of ALP activity and ARS of the BMSCs. E, F) The expression of OCN and OPN at the protein level in BMSCs after 7 days of culturing. G) RT-PCR detection of osteogenic-related gene expression in BMSCs after incubating on different samples for 4 days (Runx2 and Alp) and 7 days (Ocn, Opn, Bsp, Osx). \* $p < 0.05$ , \*\* $p < 0.01$  when compared with Ti-PtIII; # $p < 0.05$ , ## $p < 0.01$  when Ti-PtIII/PDA@ZnO-EDN1 compared with Ti-PtIII/PDA@ZnO.

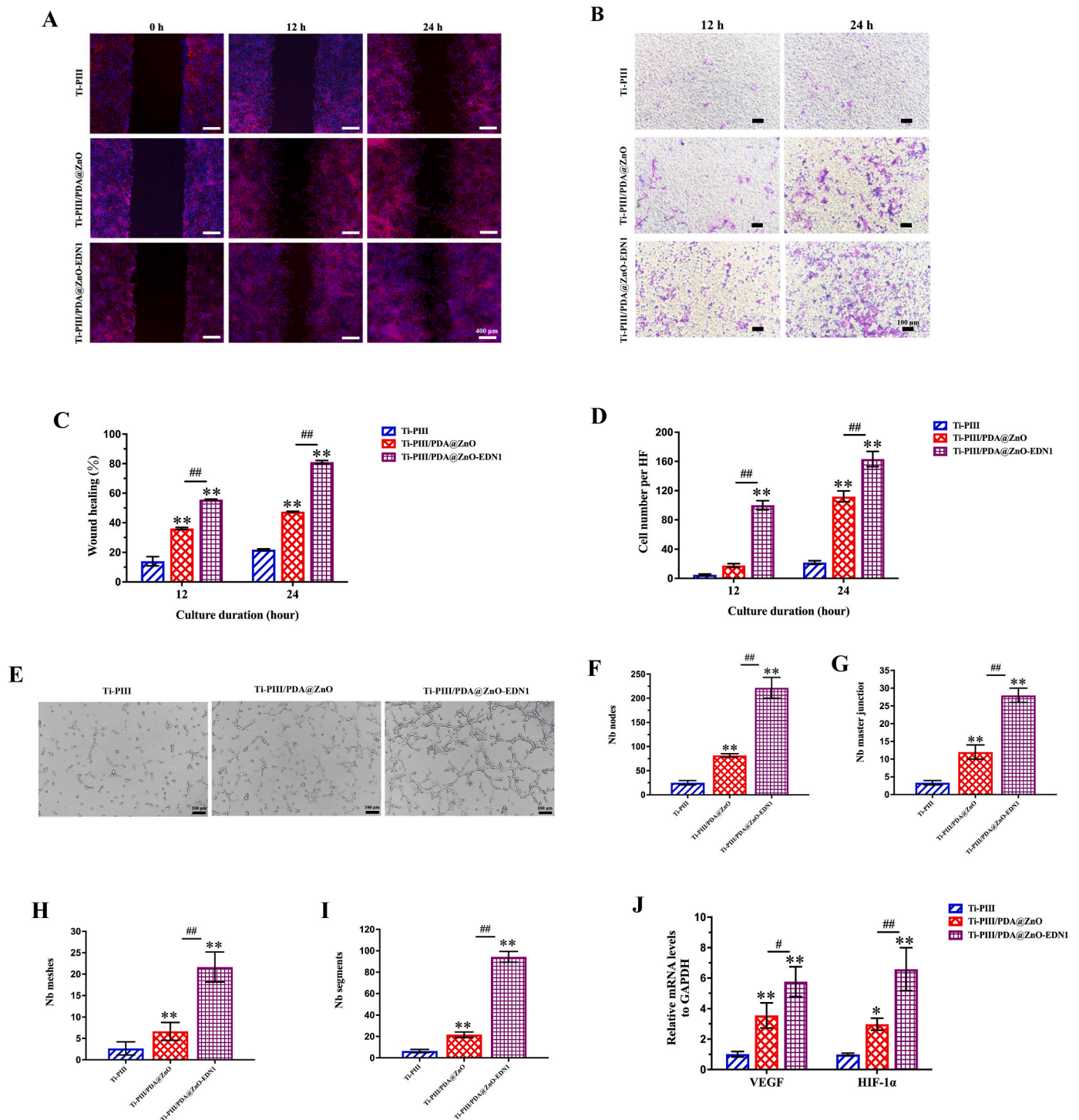


**Fig. 4.** The angiogenic effects of the modified surfaces on HUVECs. A) The migration of HUVECs on different surfaces in the wound healing assay. B) Images in the upper layers display the HUVECs penetrating the transwell membranes, under the induction of the collected culture medium for 12 and 24 h. C) The wound healing percentage. D) The statistics of the numbers of these HUVECs penetrating the transwell membranes. E) Images of the tube formation of HUVECs. F ~ I) The statistics of the numbers of the *in vitro* formed vessels. J) RT-PCR detection of VEGF and HIF-1 $\alpha$  gene expression in HUVECs after incubating on different samples for 4 days. \* $p < 0.05$ , \*\* $p < 0.01$  when compared with Ti-PIII; # $p < 0.05$ , ## $p < 0.01$  when Ti-PIII/PDA@ZnO-EDN1 compared with Ti-PIII/PDA@ZnO.

been previously reported that HIF-1 $\alpha$  facilitates osteogenesis by inducing the formation of type H vessels and promotes endothelial cell survival and maintains vascular homeostasis by upregulating the autocrine of VEGF [36,53]. Therefore, we believe that the angiogenesis inducible factors EDN1 can help recruit endothelial cells and form vascular networks in the early stage while inducing the endothelial cells to continuously release angiogenic-related factors through an autocrine

manner. With the continuous EDN1 secretion from the biomaterial surfaces, vascular maturation can eventually be realized.

#### 3.4. Assessment of antibacterial activity of the modified surfaces

It is essential for ideal implant surface to possess antibacterial activity because the implant-tissue interface is vulnerable to bacterial

attack, and uncontrolled implant infections frequently cause implant failure and require implant replacement. Initial bacterial adhesion to abiotic implant surfaces is a crucial factor in implant infection as it involves the primary stage in the biofilm formation [32,54]. Therefore, interfering with bacterial adhesion to implant surfaces at the early postoperative stage is an important strategy for achieving long-term implant success. In this work, the well-established bacteria isolated from orthopedic implant infections (*Staphylococcus aureus* (*S. aureus*) and *Escherichia coli* (*E. coli*)) were selected to assess the antibacterial effects of the modified surfaces *in vitro* and *in vivo*.

The bacterial viability was examined by the live/dead (green/red) staining assay, and the corresponding fluorescent images were shown in Fig. 5A and 5B. Compared with pristine Ti-PIII groups, there were significantly fewer bacteria attached to the modified surfaces coated with PDA@ZnO (with or without EDN1), suggesting that hybrid PDA@ZnO nanoparticles take an adhesion-resistant effect on *S. aureus* and *E. coli*. Moreover, more red but fewer green fluorescent spots were observed in Ti-PIII/PDA@ZnO and Ti-PIII/PDA@ZnO-EDN1 groups, which further indicated a superior bactericidal ability of these modified surfaces.

The contact-killing antibacterial effect against *S. aureus* and *E. coli* on different modified surfaces was further investigated by counting adherent bacteria. The adherent bacteria were detached from the samples after 6 h of incubation and then cultured on agar plates. Fig. 5C and 5D showed differences concerning the amount and viability of both *S. aureus* and *E. coli*. Fewer *S. aureus* and *E. coli* were observed in the PDA@ZnO modified groups than in the Ti-PIII group, implying a positive antibacterial effect of hybrid PDA@ZnO nanoparticles. The results of the bacteria counting assays were consistent with the live/dead staining assay discussed above. Therefore, we inferred that the multifunctional modified PEEK surface can effectively prevent bacterial adhesion and proliferation. To further confirm the contact-killing antibacterial effect, we used o-nitrophenyl- $\beta$ -D-galactopyranoside (ONPG) to examine the bacterial membrane penetrability. The ONPG can penetrate into bacteria dependent on the damage of bacterial membranes and form yellow-colored o-nitrophenol by reacting with the intracellular enzyme  $\beta$ -D-galactosidase. As shown in Fig. 5F, the permeability of the bacterial membrane was significantly increased when cultured on Ti-PIII/PDA@ZnO and Ti-PIII/PDA@ZnO-EDN1 groups. The increasing bacterial membrane penetrability was followed by intracellular content leakage including proteins and adenosine triphosphate (ATP). As expected, a decrease in ATP level was detected in bacteria cultured in two experimental groups as shown in Fig. 5G.

To better understand whether the above results were associated with the generation of ROS, we examined the decay of 1,3 Diphenylisobenzofuran (DPBF) to reveal the production of ROS. DPBF is consumed by reacting with ROS, which is embodied in a decrease of the absorption at 420 nm [55]. As shown in Fig. 5E and Fig. S5, the consumption of DPBF was significantly higher in Ti-PIII/PDA@ZnO and Ti-PIII/PDA@ZnO-EDN1 groups than the Ti-PIII group, revealing more ROS generation on the hybrid PDA@ZnO modified surfaces. We speculate that the ROS generation on modified surfaces is mainly related to the nano-oxide. Actually, the titanium energetic ions gradually undergo oxidation upon exposure to the air during the ion plasma immersion implantation, and transform into oxygen-vacant or oxygen-deficient titanium oxide [56]. ZnO NPs within the hybrid PDA@ZnO NPs modified surface also showed the presence of singly ionized oxygen vacancy (i.e. oxygen vacancy with one electron). Oxygen from the atmosphere can react with an electron from the ZnO NPs surface to form a superoxide radical [57]. Oxygen vacancies in TiO<sub>2</sub> and ZnO are so highly reactive that ROS are successively produced in the microenvironment to damage the bacteria surface causing cell death [56,58].

In conclusion, potential antibacterial mechanisms of our PDA@ZnO modified substrates are listed as follows: (a) ROS damage the intracellular contents including proteins, DNA, ATP, etc. through intense oxidative stress reactions after being internalized into the bacterial cell

membrane. (b) Zinc ions released from the ZnO nanoparticles can cause mechanical damage to the bacterial cell wall, thus penetrating cell membranes to inhibit active transport and glucose metabolism and disrupt metal ion homeostasis and enzyme systems when the concentration reaches a specific level. (c) ZnO nanoparticles directly contact bacterial cell walls, causing damage to the membrane integrity and subsequent death.

### 3.5. Bone formation evaluation and histopathological evaluation *in vivo*

#### 3.5.1. Antibacterial efficiency and biosafety assessment *in vivo*

In the present study, we employed the rat femoral condyle model of implant infection to characterize the *in vivo* biological behaviors of different modified implants. After 6 weeks of implantation, the rats were sacrificed and implants were taken out to count the residual bacteria. As shown in Fig. 6A and 6B, severe implant infections occurred on Ti-PIII implants as a large number of bacteria were detected. By contrast, PDA@ZnO modified samples showed excellent antibacterial activity with few bacteria detected. In addition, large numbers of inflammatory cells were observed around Ti-PIII implants while PDA@ZnO modified implants were infiltrated by few inflammatory cells according to hematoxylin and eosin (H&E) staining images (red arrow in Fig. 6C). The results revealed that the immobilized hybrid PDA@ZnO nanoparticles could inhibit severe inflammatory responses, thereby endowing CFRPEEK implants with excellent *in vivo* antibacterial activities.

The *in vivo* biosafety of the multifunctional implant was also detected by H&E staining. According to the histological images (Fig. 6D), there was no evidence of pathological abnormalities in any examined rat major metabolic organs (including heart, liver, spleen, lung and kidney), revealing good biosafety of the nanoparticles decorated PEEK implants.

#### 3.5.2. Bone formation evaluation and histopathological evaluation *in vivo*

CT scan images of rat femoral bones after 6 weeks of implantation from all three groups were shown in Fig. 7A. From the 2D images, we can observe more bones were formed in the marrow cavity of PDA@ZnO modified samples. The bone volume around the Ti-PIII/PDA@ZnO-EDN1 group was the largest among the three groups. The reconstructed 3D images of Ti-PIII, Ti-PIII/PDA@ZnO, and Ti-PIII/PDA@ZnO-EDN1 showed the same trend, with the more new bone formation on the EDN1 modified surface (Fig. 7A–C).

The detail of the bone-implant interface (Fig. 7E) was shown on Van Gieson's picrofuchsin staining sections (Fig. 7F). In the Ti-PIII group, the obvious interspace between the newly formed bone and the implant surface was filled with fibrous tissue. By comparison, more dense newly grown bones closed to the implant surfaces exhibited in EDN1 conjugated groups. As we know, the percentage of bone-implant contact (BIC) and the peri-implant bone area are two vital factors contributing to the quality of osseointegration. Both the BIC (Fig. 7G) and the area of new bone (Fig. 7H) in the EDN1 group were significantly higher than the other two groups. Taking all these results together, the PDA@ZnO-EDN1 coating has driven the osseointegration to a high level in a short time.

Interestingly, sequence fluorescence (Fig. 7J and 7K) showed that there was continuous red fluorescence deposition close to the EDN1-decorated implant surface at 2 weeks after implantation, while the red fluorescence of the other two groups was significantly weaker, which showed that the PDA@ZnO-EDN1 modified implant could effectively stimulate early bone formation. This may be related to the multifunctional surface promoting the adhesion and osteogenic differentiation of stem cells on its surface. In addition, the released Zn ions and EDN1 *in vivo* might also play a remote action that induces angiogenesis and osteogenesis in the gap between the implant surface and host bones as shown in the Scheme, to promote rapid new bone formation which could be supported by the more active mineralization around the implants in the Ti-PIII/PDA@ZnO-EDN1 group at both observation time points (2 and 4 weeks).

We further characterized the vascularization of the implants by

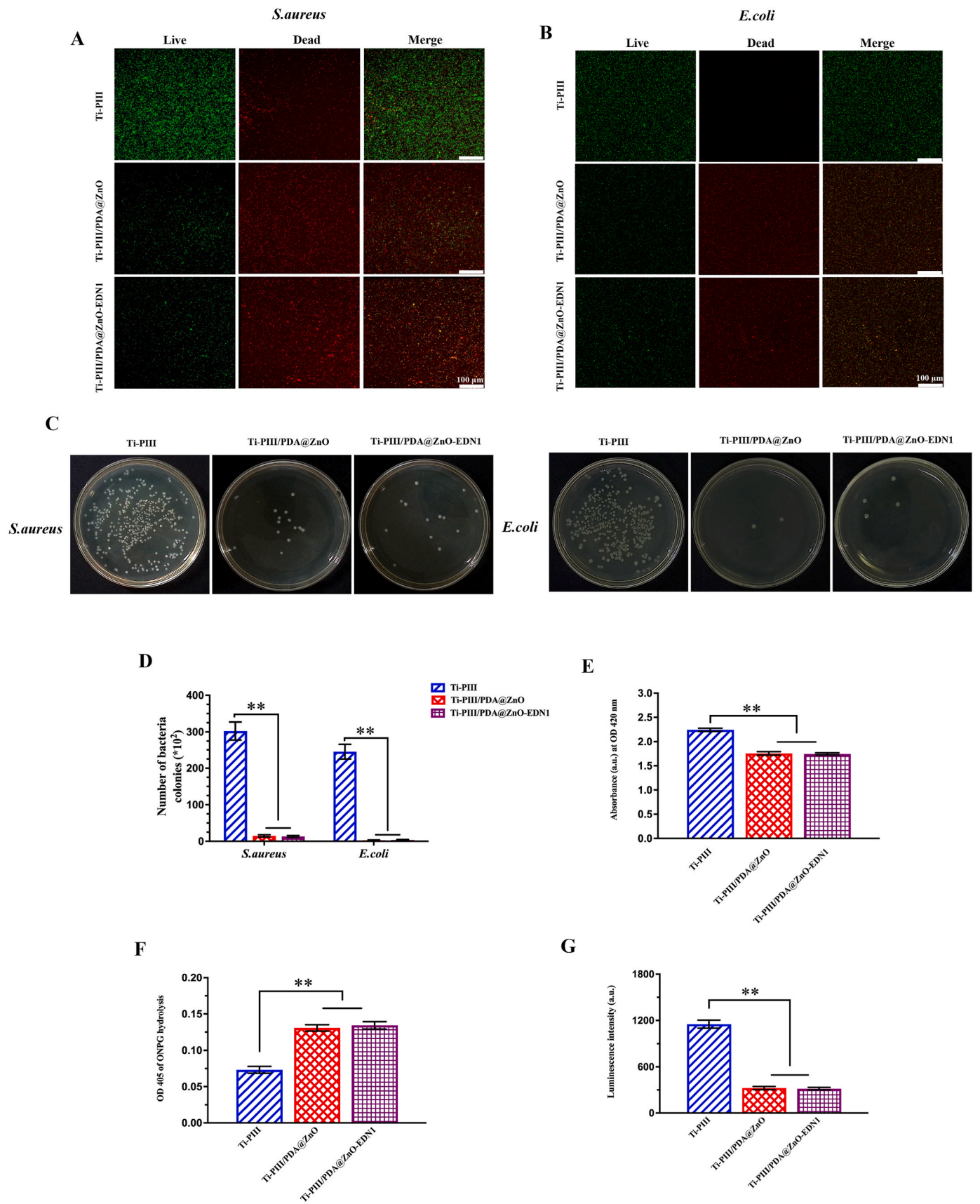


**Fig. 5.** Investigation of antibacterial effects. A, B) Confocal micrographs of bacteria cultured on samples for 12 h, the green fluorescence referred to live bacteria and red referred to dead bacteria. C, D) Numbers of bacteria colonies adhered to different groups for *S. aureus* and *E. coli*. E) ROS detected through detecting the decay of DPBF when incubated with different samples. F) *S. aureus* membrane permeability assessed by ONPG hydrolysis assay. G) Cellular ATP level of *S. aureus* reflected by luminescence intensity after different treatments. \* $p < 0.05$ , \*\* $p < 0.01$  when compared with Ti-PHII.

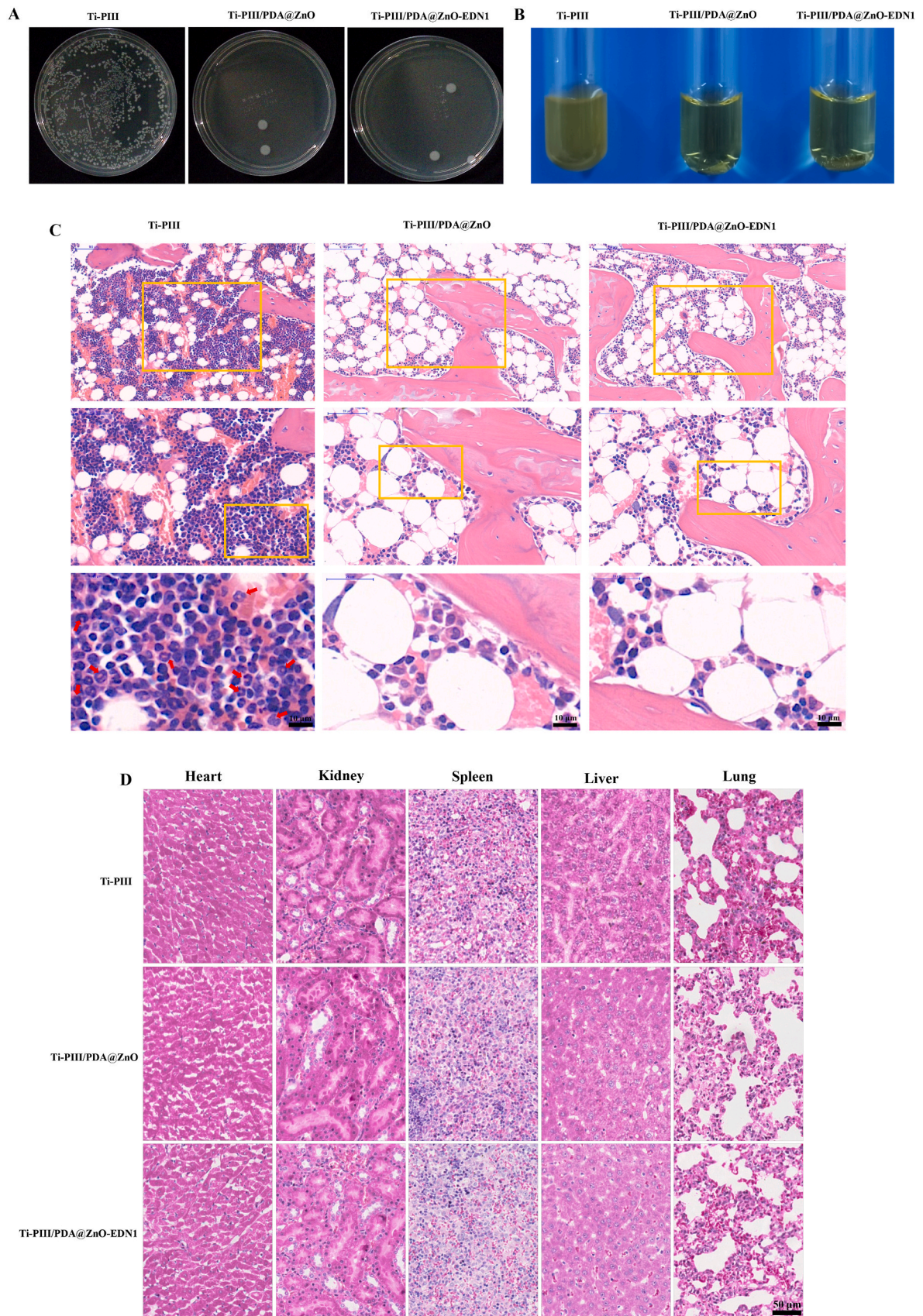


**Fig. 6.** Evaluation of *in vivo* antibacterial effects. A) Photograph of bacteria colonies plates of different samples taken from different rats. B) Photograph of bacteria culture mediums of different samples taken from different rats. C) Infection degree around different implants assessed by H&E staining. Red arrows represented lobulated neutrophils. D) H&E staining images of major organs (including heart, kidney, spleen, liver, lung) collected from different samples implanted in rats.

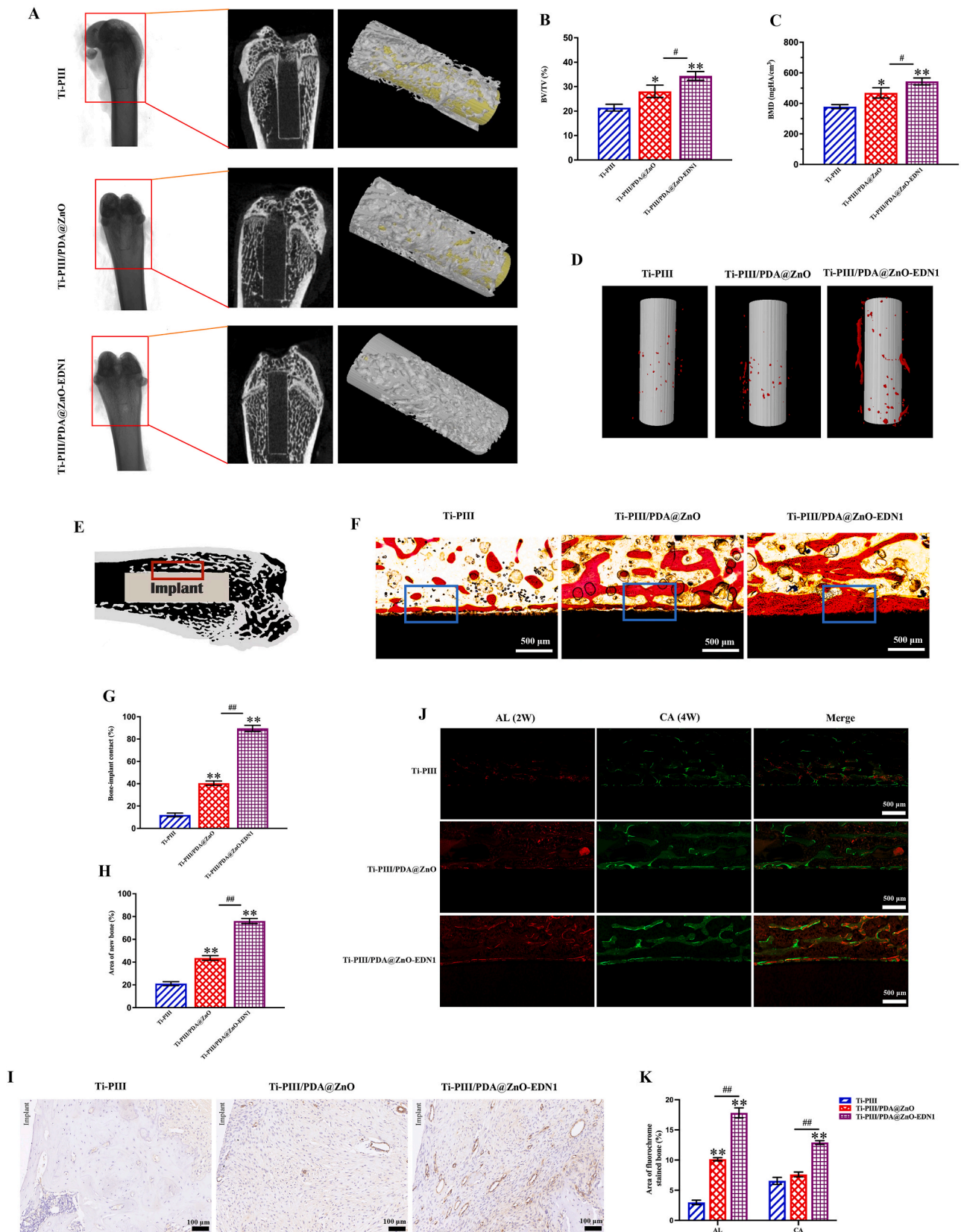


**Fig. 7.** Multifunctional implants promoted vascularized rapid osseointegration *in vivo*. A) Characterization of implants and the surrounding bones by Micro-CT. B, C) Quantitative analysis of the percentage of bone volume to tissue volume (BV/TV), new bone mineral density. D) Angiography around implants by Micro-CT. E) Schematic view of the implant in rat femur bones. The red rectangular area indicated the histological observation region. F) Histological sections stained with Van Gieson's picrofuchsin solution. G, H) The statistical results of the percent of BIC and the area of newly-formed bones around the implants. I) The histological sections stained of CD31. J) Sequential fluorescent labeling observations. K) The statistical results of the fluorochrome area. \* $p < 0.05$ , \*\* $p < 0.01$  when compared with Ti-PIII; # $p < 0.05$ , ## $p < 0.01$  when Ti-PIII/PDA@ZnO-EDN1 compared with Ti-PIII/PDA@ZnO.

Micro-CT and CD31 immunohistochemistry. The results of the new vessel formation around implants were presented by Micro-CT as shown in Fig. 7D, suggesting that the amount of blood vessel growth in the EDN1 modified group was markedly larger than the other two groups. Similarly, the expression of CD31 protein in the Ti-PIII/PDA@ZnO-EDN1 group was also significantly increased (Fig. 7I).

#### 4. Conclusions

In summary, this study not only provides valuable information on the biological interaction of PDA@ZnO-EDN1 decorated CFRPEEK implants with BMSCs, HUVECs, bacteria, and host osseous tissue but also further reaches advancements for bacterial infection-associated orthopedic implantation. As taking the strategy of incorporating hybrid PDA@ZnO nanoparticles and the active factor EDN1 onto CFRPEEK implants, an efficient antibacterial treatment was also achieved. Hence, our Ti-PIII/PDA@ZnO-EDN1 CFRPEEK implants provide a promising solution for the application of PEEK materials in the field of orthopedic and dentistry.

#### Ethical approval

All institutional and national guidelines for the care and use of laboratory animals were followed. All experimental protocols involving animals were approved by the Institutional Animal Care and Use Committee and followed the procedure for Animal Experimental Ethical Inspection of the Ninth People's Hospital, which is affiliated with Shanghai Jiao Tong University School of Medicine (SCXK [Shanghai] [201866]).

#### Author declaration

We wish to confirm that there are no known conflicts of interest associated with this publication and there has been no significant financial support for this work that could have influenced its outcome.

#### CRedit authorship contribution statement

**Xiao Wang:** Conceptualization, Methodology, Formal analysis, Writing – original draft. **Lisha Pan:** Methodology, Investigation, Writing – original draft. **Ao Zheng:** Methodology, Validation. **Lingyan Cao:** Formal analysis, Validation. **Jin Wen:** Data curation, Resources. **Tingshu Su:** Writing – original draft, Validation. **Xiangkai Zhang:** Resources, Investigation. **Qingfeng Huang:** Resources, Conceptualization, Funding acquisition. **Xinquan Jiang:** Conceptualization, Methodology, Supervision, Writing – review & editing, Funding acquisition.

#### Declaration of competing interest

The authors declare that they have no known competing financial interests or personal relationships that could have appeared to influence the work reported in this paper.

#### Acknowledgments

This work was funded by the National Natural Science Foundation of China (No. 81921002, No. 82100963, No. 81873709), the Natural Science Foundation of Shanghai Science and Technology Commission (21ZR1437100), Shanghai Rising-Star Program (21QA1405400).

#### Appendix A. Supplementary data

Supplementary data to this article can be found online at <https://doi.org/10.1016/j.bioactmat.2022.12.016>.

#### References

- [1] T. Krätzig, K.C. Mende, M. Mohme, H. Kniep, M. Dreimann, M. Stangenberg, M. Westphal, T. Gauer, S.O. Eicker, Carbon fiber-reinforced PEEK versus titanium implants: an in vitro comparison of susceptibility artifacts in CT and MR imaging, *Neurosurg. Rev.* 44 (4) (2021) 2163–2170.
- [2] S.M. Kurtz, J.N. Devine, PEEK biomaterials in trauma, orthopedic, and spinal implants, *Biomaterials* 28 (32) (2007) 4845–4869.
- [3] S. Wang, Y. Yang, Y. Li, J. Shi, J. Zhou, L. Zhang, Y. Deng, W. Yang, Strontium/adiponectin co-decoration modulates the osteogenic activity of nano-morphologic polyetheretherketone implant, *Colloids Surf. B Biointerfaces* 176 (2019) 38–46.
- [4] L. Qin, S. Yao, J. Zhao, C. Zhou, T.W. Oates, M.D. Weir, J. Wu, H.H.K. Xu, Review on development and dental applications of polyetheretherketone-based biomaterials and restorations, *Materials* 14 (2) (2021) 408.
- [5] T. Lu, J. Li, S. Qian, H. Cao, C. Ning, X. Liu, Enhanced osteogenic and selective antibacterial activities on micro-/nano-structured carbon fiber reinforced polyetheretherketone, *J. Mater. Chem. B* 4 (17) (2016) 2944–2953.
- [6] M.B. da Cruz, J.F. Marques, G.M. Peñarrieta-Juanito, M. Costa, J.C.M. Souza, R. S. Magini, G. Miranda, F.S. Silva, J.M.M. Caramés, A. da Mata, Bioactive-enhanced polyetheretherketone dental implant materials: mechanical characterization and cellular responses, *J. Oral Implantol.* 47 (1) (2021) 9–17.
- [7] W. Yu, H. Zhang, L. A. S. Yang, J. Zhang, H. Wang, Z. Zhou, Y. Zhou, J. Zhao, Z. Jiang, Enhanced bioactivity and osteogenic property of carbon fiber reinforced polyetheretherketone composites modified with amino groups, *Colloids Surf. B Biointerfaces* 193 (2020), 111098.
- [8] W. Liu, J. Li, M. Cheng, Q. Wang, Y. Qian, K.W.K. Yeung, P.K. Chu, X. Zhang, A surface-engineered polyetheretherketone biomaterial implant with direct and immunoregulatory antibacterial activity against methicillin-resistant *Staphylococcus aureus*, *Biomaterials* 208 (2019) 8–20.
- [9] C. Yang, L. Ouyang, W. Wang, B. Chen, W. Liu, X. Yuan, Y. Luo, T. Cheng, K.W. K. Yeung, X. Liu, X. Zhang, Sodium butyrate-modified sulfonated polyetheretherketone modulates macrophage behavior and shows enhanced antibacterial and osteogenic functions during implant-associated infections, *J. Mater. Chem. B* 7 (36) (2019) 5541–5553.
- [10] T. Chen, Q. Chen, H. Fu, D. Wang, Y. Gao, M. Zhang, H. Liu, Construction and performance evaluation of a sustained release implant material polyetheretherketone with antibacterial properties, *Mater Sci Eng C Mater Biol Appl* 126 (2021), 112109.
- [11] X. Shen, Y. Zhang, P. Ma, L. Sutrisno, Z. Luo, Y. Hu, Y. Yu, B. Tao, C. Li, K. Cai, Fabrication of magnesium/zinc-metal organic framework on titanium implants to inhibit bacterial infection and promote bone regeneration, *Biomaterials* 212 (2019) 1–16.
- [12] G. Wang, W. Jin, A.M. Qasim, A. Gao, X. Peng, W. Li, H. Feng, P.K. Chu, Antibacterial effects of titanium embedded with silver nanoparticles based on electron-transfer-induced reactive oxygen species, *Biomaterials* 124 (2017) 25–34.
- [13] M. Li, Z. Ma, Y. Zhu, H. Xia, M. Yao, X. Chu, X. Wang, K. Yang, M. Yang, Y. Zhang, C. Mao, Toward a molecular understanding of the antibacterial mechanism of copper-bearing titanium alloys against *Staphylococcus aureus*, *Adv Healthc Mater* 5 (5) (2016) 557–566.
- [14] K. Yonezawa, M. Kawaguchi, A. Kaneuji, T. Ichiseki, Y. Inuma, K. Kawamura, K. Shintani, S. Oda, M. Taki, N. Kawahara, Evaluation of antibacterial and cytotoxic properties of a fluorinated diamond-like carbon coating for the development of antibacterial medical implants, *Antibiotics (Basel)* 9 (8) (2020).
- [15] S.M. Skovdøl, N.P. Jørgensen, E. Petersen, S. Jensen-Fangel, R. Ogaki, G. Zeng, M. I. Johansen, M. Wang, H. Rohde, R.L. Meyer, Ultra-dense polymer brush coating reduces *Staphylococcus epidermidis* biofilms on medical implants and improves antibiotic treatment outcome, *Acta Biomater.* 76 (2018) 46–55.
- [16] S.J. Lee, D.N. Heo, H.R. Lee, D. Lee, S.J. Yu, S.A. Park, W.K. Ko, S.W. Park, S.G. Im, J.H. Moon, I.K. Kwon, Biofunctionalized titanium with anti-fouling resistance by grafting thermo-responsive polymer brushes for the prevention of peri-implantitis, *J. Mater. Chem. B* 3 (26) (2015) 5161–5165.
- [17] Q. Gao, M. Yu, Y. Su, M. Xie, X. Zhao, P. Li, P.X. Ma, Rationally designed dual functional block copolymers for bottlebrush-like coatings: in vitro and in vivo antimicrobial, antibiofilm, and antifouling properties, *Acta Biomater.* 51 (2017) 112–124.
- [18] A. Valverde, L. Pérez-Álvarez, L. Ruiz-Rubio, M.A. Pacha Olivenza, M.B. García Blanco, M. Díaz-Fuentes, J.L. Vilas-Vilela, Antibacterial hyaluronic acid/chitosan multilayers onto smooth and micropatterned titanium surfaces, *Carbohydr. Polym.* 207 (2019) 824–833.
- [19] R. Brayner, R. Ferrari-Iliou, N. Brivois, S. Djediat, M.F. Benedetti, F. Fiévet, Toxicological impact studies based on *Escherichia coli* bacteria in ultrafine ZnO nanoparticles colloidal medium, *Nano Lett.* 6 (4) (2006) 866–870.
- [20] K.M. Reddy, K. Feris, J. Bell, D.G. Wingett, C. Hanley, A. Punnoose, Selective toxicity of zinc oxide nanoparticles to prokaryotic and eukaryotic systems, *Appl. Phys. Lett.* 90 (213902) (2007) 213902–2139023.
- [21] C. Hanley, J. Layne, A. Punnoose, K.M. Reddy, I. Coombs, A. Coombs, K. Feris, D. Wingett, Preferential killing of cancer cells and activated human T cells using ZnO nanoparticles, *Nanotechnology* 19 (29) (2008), 295103.
- [22] N. Padmavathy, R. Vijayaraghavan, Enhanced bioactivity of ZnO nanoparticles-an antimicrobial study, *Sci. Technol. Adv. Mater.* 9 (3) (2008), 035004.
- [23] A. Sirelkhatim, S. Mahmud, A. Seeni, N.H.M. Kaus, L.C. Ann, S.K.M. Bakhori, H. Hasan, D. Mohamad, Review on zinc oxide nanoparticles: antibacterial activity and toxicity mechanism, *Nano-Micro Lett.* 7 (3) (2015) 219–242.
- [24] Y. Li, Y. Yang, Y. Qing, R. Li, X. Tang, D. Guo, Y. Qin, Enhancing ZnO-NP antibacterial and osteogenesis properties in orthopedic applications: a review, *Int. J. Nanomed.* 15 (2020) 6247–6262.

- [25] Z. Wang, X. Wang, Y. Wang, Y. Zhu, X. Liu, Q. Zhou, NanoZnO-modified titanium implants for enhanced anti-bacterial activity, osteogenesis and corrosion resistance, *J. Nanobiotechnol.* 19 (1) (2021) 353.
- [26] K.B. Hadley, S.M. Newman, J.R. Hunt, Dietary zinc reduces osteoclast resorption activities and increases markers of osteoblast differentiation, matrix maturation, and mineralization in the long bones of growing rats, *J. Nutr. Biochem.* 21 (4) (2010) 297–303.
- [27] A.P.S. Prasanna, K.S. Venkataprasanna, B. Pannervelam, V. Asokan, R.S. Jeniffer, G.D. Venkatasubbu, Multifunctional ZnO/SiO<sub>2</sub> core/shell nanoparticles for bioimaging and drug delivery application, *J. Fluoresc.* 30 (5) (2020) 1075–1083.
- [28] S.B. Ghaffari, M.H. Sarrafzadeh, M. Salami, M.R. Khorramizadeh, A pH-sensitive delivery system based on N-succinyl chitosan-ZnO nanoparticles for improving antibacterial and anticancer activities of curcumin, *Int. J. Biol. Macromol.* 151 (2020) 428–440.
- [29] W. Song, J. Zhang, J. Guo, J. Zhang, F. Ding, L. Li, Z. Sun, Role of the dissolved zinc ion and reactive oxygen species in cytotoxicity of ZnO nanoparticles, *Toxicol. Lett.* 199 (3) (2010) 389–397.
- [30] S.A. James, B.N. Feltis, M.D. de Jonge, M. Sridhar, J.A. Kimpton, M. Altissimo, S. Mayo, C. Zheng, A. Hastings, D.L. Howard, D.J. Paterson, P.F. Wright, G. F. Moorhead, T.W. Turney, J. Fu, Quantification of ZnO nanoparticle uptake, distribution, and dissolution within individual human macrophages, *ACS Nano* 7 (12) (2013) 10621–10635.
- [31] N. Adam, C. Schmitt, J. Galceran, E. Companys, A. Vakurov, R. Wallace, D. Knapen, R. Blust, The chronic toxicity of ZnO nanoparticles and ZnCl<sub>2</sub> to *Daphnia magna* and the use of different methods to assess nanoparticle aggregation and dissolution, *Nanotoxicology* 8 (7) (2014) 709–717.
- [32] C.R. Ariola, D. Campoccia, L. Montanaro, Implant infections: adhesion, biofilm formation and immune evasion, *Nat. Rev. Microbiol.* 16 (7) (2018) 397–409.
- [33] L. Le Guehennec, A. Soueidan, P. Layrolle, Y. Amouriq, Surface treatments of titanium dental implants for rapid osseointegration, *Dent. Mater.* 23 (7) (2007) 844–854.
- [34] P.I. Brånemark, R. Adell, U. Breine, B.O. Hansson, J. Lindström, A. Ohlsson, Intraosseous anchorage of dental prostheses. I. Experimental studies, *Scand. J. Plast. Reconstr. Surg.* 3 (2) (1969) 81–100.
- [35] T. Albrektsson, G. Zarb, P. Worthington, A.R. Eriksson, The long-term efficacy of currently used dental implants: a review and proposed criteria of success, *Int. J. Oral Maxillofac. Implants* 1 (1) (1986) 11–25.
- [36] A.P. Kusumbe, S.K. Ramasamy, R.H. Adams, Coupling of angiogenesis and osteogenesis by a specific vessel subtype in bone, *Nature* 507 (7492) (2014) 323–328.
- [37] S.K. Ramasamy, A.P. Kusumbe, L. Wang, R.H. Adams, Endothelial Notch activity promotes angiogenesis and osteogenesis in bone, *Nature* 507 (7492) (2014) 376–380.
- [38] L.H. Nguyen, N. Annabi, M. Nikkha, H. Bae, L. Binan, S. Park, Y. Kang, Y. Yang, A. Khademhosseini, Vascularized bone tissue engineering: approaches for potential improvement, *Tissue Eng. B Rev.* 18 (5) (2012) 363–382.
- [39] M.I. Santos, R.L. Reis, Vascularization in bone tissue engineering: physiology, current strategies, major hurdles and future challenges, *Macromol. Biosci.* 10 (1) (2010) 12–27.
- [40] M. Yanagisawa, H. Kurihara, S. Kimura, Y. Tomobe, M. Kobayashi, Y. Mitsui, Y. Yazaki, K. Goto, T. Masaki, A novel potent vasoconstrictor peptide produced by vascular endothelial cells, *Nature* 332 (6163) (1988) 411–415.
- [41] D. Salani, G. Taraboletti, L. Rosanò, V. Di Castro, P. Borsotti, R. Giavazzi, A. Bagnato, Endothelin-1 induces an angiogenic phenotype in cultured endothelial cells and stimulates neovascularization in vivo, *Am. J. Pathol.* 157 (5) (2000) 1703–1711.
- [42] T.L. Tsai, B. Wang, M.W. Squire, L.W. Guo, W.J. Li, Endothelial cells direct human mesenchymal stem cells for osteo- and chondro-lineage differentiation through endothelin-1 and AKT signaling, *Stem Cell Res. Ther.* 6 (1) (2015) 88.
- [43] L.W. Hu, X. Wang, X.Q. Jiang, L.Q. Xu, H.Y. Pan, In vivo and in vitro study of osteogenic potency of endothelin-1 on bone marrow-derived mesenchymal stem cells, *Exp. Cell Res.* 357 (1) (2017) 25–32.
- [44] H. Lee, S.M. Dellatore, W.M. Miller, P.B. Messersmith, Mussel-inspired surface chemistry for multifunctional coatings, *Science* 318 (5849) (2007) 426–430.
- [45] Y. Liu, K. Ai, L. Lu, Polydopamine and its derivative materials: synthesis and promising applications in energy, environmental, and biomedical fields, *Chem. Rev.* 114 (9) (2014) 5057–5115.
- [46] W. Zhang, Y. Jin, S. Qian, J. Li, Q. Chang, D. Ye, H. Pan, M. Zhang, H. Cao, X. Liu, X. Jiang, Vacuum extraction enhances rhPDGF-BB immobilization on nanotubes to improve implant osseointegration in ovariectomized rats, *Nanomedicine* 10 (8) (2014) 1809–1818.
- [47] T. Svitkina, The actin cytoskeleton and actin-based motility, *Cold Spring Harbor Perspect. Biol.* 10 (1) (2018).
- [48] X. Wang, T. Lu, J. Wen, L. Xu, D. Zeng, Q. Wu, L. Cao, S. Lin, X. Liu, X. Jiang, Selective responses of human gingival fibroblasts and bacteria on carbon fiber reinforced polyetheretherketone with multilevel nanostructured TiO<sub>2</sub>, *Biomaterials* 83 (2016) 207–218.
- [49] S. Oh, K.S. Brammer, Y.S. Li, D. Teng, A.J. Engler, S. Chien, S. Jin, Stem cell fate dictated solely by altered nanotube dimension, *Proc. Natl. Acad. Sci. U. S. A.* 106 (7) (2009) 2130–2135.
- [50] J. Park, S. Bauer, K.A. Schlegel, F.W. Neukam, K. von der Mark, P. Schmuki, TiO<sub>2</sub> nanotube surfaces: 15 nm—an optimal length scale of surface topography for cell adhesion and differentiation, *Small* 5 (6) (2009) 666–671.
- [51] J. Park, S. Bauer, K. von der Mark, P. Schmuki, Nanosize and vitality: TiO<sub>2</sub> nanotube diameter directs cell fate, *Nano Lett.* 7 (6) (2007) 1686–1691.
- [52] K.S. Brammer, S. Oh, C.J. Cobb, L.M. Bjursten, H. van der Heyde, S. Jin, Improved bone-forming functionality on diameter-controlled TiO<sub>2</sub> nanotube surface, *Acta Biomater.* 5 (8) (2009) 3215–3223.
- [53] S. Lee, T.T. Chen, C.L. Barber, M.C. Jordan, J. Murdock, S. Desai, N. Ferrara, A. Nagy, K.P. Roos, M.L. Iruela-Arispe, Autocrine VEGF signaling is required for vascular homeostasis, *Cell* 130 (4) (2007) 691–703.
- [54] M. Chen, L. Ouyang, T. Lu, H. Wang, F. Meng, Y. Yang, C. Ning, J. Ma, X. Liu, Enhanced bioactivity and bacteriostasis of surface fluorinated polyetheretherketone, *ACS Appl. Mater. Interfaces* 9 (20) (2017) 16824–16833.
- [55] H. Wang, X. Yang, W. Shao, S. Chen, J. Xie, X. Zhang, J. Wang, Y. Xie, Ultrathin black phosphorus nanosheets for efficient singlet oxygen generation, *J. Am. Chem. Soc.* 137 (35) (2015) 11376–11382.
- [56] P.C. Maness, S. Smolinski, D.M. Blake, Z. Huang, E.J. Wolfrum, W.A. Jacoby, Bactericidal activity of photocatalytic TiO<sub>2</sub> reaction: toward an understanding of its killing mechanism, *Appl. Environ. Microbiol.* 65 (9) (1999) 4094–4098.
- [57] L. Oleg, C. Lee, C. Guangyu, A single ZnO tetrapod-based sensor, *Sensor. Actuator. B Chem.* 141 (2) (2009) 511–517.
- [58] L. Zhang, Y. Jiang, Y. Ding, M. Povey, D. York, Investigation into the antibacterial behaviour of suspensions of ZnO nanoparticles (ZnO nanofluids), *J. Nanoparticle Res.* 9 (3) (2007) 479–489.